Incommensurate Moiré overlayer with strong local binding: CoO(111) bilayer on Ir(100)

C. Tröppner, T. Schmitt, M. Reuschl, L. Hammer, M. A. Schneider, F. Mittendorfer, J. Redinger, R. Podloucky, and M. Weinert

Phys. Rev. B **86**, 235407 — Published 6 December 2012

DOI: 10.1103/PhysRevB.86.235407

An incommensurate Moiré overlayer with strong local binding: CoO(111) bilayer on Ir(100)

C. Tröppner, T. Schmitt, M. Reuschl, L. Hammer, and M.A. Schneider*
Chair of Solid State Physics, University Erlangen-Nuremberg, Staudtstr. 7, D-91058 Erlangen, Germany

F. Mittendorfer and J. Redinger
Inst. of Applied Physics, Vienna University of Technology, Gusshausstr. 25/13, A-1040 Vienna, Austria

R. Podloucky
Inst. of Physical Chemistry, Vienna University, Sensengasse 8, A-1090 Vienna, Austria

M. Weinert
Dept. of Physics, University of Wisconsin-Milwaukee, Milwaukee, WI 53201, USA
(Dated: November 20, 2012)

Incommensurate relaxed overlayer Moiré structures are often interpreted as systems with weak lateral variations of the binding potential and thus no structural modulations in the overlayer material. We discuss here the example of a CoO(111) bilayer on Ir(100), which is a relaxed overlayer with strong structural response to the lateral modulation of interface properties but nevertheless is incommensurate. By means of DFT calculations we quantitatively reproduce all the structural parameters of the CoO(111) bilayer on Ir(100) as proposed by a recent LEED analysis [C. Ebensperger et al., Phys. Rev. B 81, 235405 (2010)]. The calculations predict energetic degeneracies with respect to registry shifts of the CoO(111) film along $[01\bar{1}]$. Large-scale, low-temperature STM topographies reveal that the true structure of the film is incommensurate in this direction, exhibiting a one-dimensional Moiré pattern with a period of about 9.4 a_{Ir}. From DFT calculations for limiting (periodic) models, we can sample the potential landscape of the cobalt and oxygen atoms in the Moiré structure across the Ir(100) unit cell. We find that despite the non-commensurability of the film, the binding to the substrate is site specific with strong attraction and repulsion points for both cobalt and oxygen atoms, leading to severe local distortions in the film. The lateral modulation of the structural elements within the oxide film can be understood as a combination of the lateral variation in the Co-Ir binding potential and additional O-Ir binding.

I. INTRODUCTION

Oxides of transition metals such as Fe, Mn, or Co are of interest both for fundamental reasons and for technological applications. Cobalt oxide especially has the potential to play a key role in the fields of catalysis, sensors, battery technology, and nanomagnetic applications.[1–6] The downsizing of oxide materials to nanometer dimensions may lead to properties strongly deviating compared to those of bulk.[7–10] Ultra-thin oxide films supported on a metal substrate additionally suffer from the inhomogeneous chemical binding at the interface, arising from the different lateral periodicities of film and substrate. As a result, the imposed stress induces local structural distortions and frequently also bond breaking events. Even completely new crystallographic structures unknown from bulk physics may be stabilized.[9] Therefore, a targeted use of such materials requires a detailed understanding of their crystallographic and electronic structure at the atomic level. The influence of the supporting metal can be investigated by considering ultra-thin oxide films that are basically slabs of the bulk structure, such that the distortions are exclusively due to interface accommodation. Candidates are rock-salt type FeO, MnO, and CoO films of (111) orientation, for which films of ultimate thinness — single hexagonal metal-oxygen bilayers — have been found on a number of metal substrates.[11–20] In these cases high-order commensurate phases were reported with unit cell dimensions of about ten times that of the substrate, corresponding to about 10% lattice misfits between substrates and oxide films. In the case of (100) oriented substrates, this just leads to close correspondence of row distances in one direction and, by a slight uniaxial distortion, the films achieve one-dimensional commensurability (row-on-row matching).

The common long-range periodicity of the whole system (film plus substrate) may alternatively be described as a Moiré-like superposition of the different lattices involved. The description by means of a Moiré period has the advantage that it does not require a common multiple of lattice vectors, as is the case for a commensurate superstructure. As a consequence, slight deviations in size or orientation of the film due to details of the preparation (island sizes, defect density etc.)[15] or simply the limited resolution of the applied real or reciprocal space methods will not lead to totally different notations such as, for example, FeO on Pt(111) (10×10),[11] $(\sqrt{84} \times \sqrt{84})R10.9°$,[14] and $(\sqrt{91} \times \sqrt{91})R5.2°$.[14,15])

The structure of Moiré-like films are often regarded as approximately sinusoidal waves with constant bond lengths at the interface (hard-sphere model). This view, however, requires laterally unspecified binding properties of the film to the substrate, i.e., an uncorrugated binding potential, an approximation which may not be valid in all cases. Such a situation was demonstrated in a recent full-dynamical low-energy electron diffraction (LEED) analysis[19] of a CoO bilayer film grown on Ir(100): For the c(10×2) structure, a particularly unusual geometry was determined showing enormous height differences of up to 1 Å between the oxygen atoms at the vacuum side of the structure and of 0.5 Å between the cobalt atoms at the interface. These height differences are much larger than the predictions of a hard-sphere model. Confirming this unusual structural model, recent ab-initio calculations[21] also predict strain- and structure-driven complex magnetic ordering of the CoO overlayer on Ir(100). A close relationship between the local structural properties of the oxide film and the induced magnetic order was found, leading to alternating ferromagnetically and antiferromagnetically ordered segments. Interestingly, a second energetically almost degenerate c(10×2) structure was also found, related to the former by a registry shift of the CoO overlayer. These findings are in contrast to a recent study for the closely related system of a CoO bilayer on Pd(100) with (9×2) periodicity, for which only a moderately corrugated structure (height modulations of 0.18 Å and 0.12 Å for the oxygen and cobalt, respectively) was reported.[20] Similarly small corrugations were also reported for the FeO bilayer on Pt(111).[14] The aim of the present study is to test the extent to which the parameters of the DFT calculation and the magnetic order of the film influence the correspondence between the calculated and the experimentally determined structure. Further, we investigate which atomic species are imaged in scanning tunneling microscopy (STM) topographies, whether the assignment depends on the interface registry, as in the case of FeO on Pt(111),[14] and clarify (through the use of low-temperature STM imaging) how the proposed degeneracy of the film with respect to the registry with the substrate is reflected in its real-space structure.

In brief, we find that the experimental determination of the CoO bilayer structure on Ir(100) is indeed correct, but there are energetically degenerate configurations possible and that the calculated structure — and hence agreement with experiment — depends on the magnetic order of the Co atoms. By virtue of large scale topographies with atomic resolution taken by low-temperature STM, we can identify the local registry of the film with the substrate and find the proposed energetically degenerate configurations. Thus, the c(10×2) film structure is only an approximation to the one-dimensional Moiré structure the film adopts, i.e., neighboring c(10×2) cells probe slightly different local configurations with respect to the substrate. Using the structural results of the fully relaxed DFT models, we can sample the positions of both the oxygen and cobalt species across the substrate unit cell and thus identify pronounced local extrema in the binding potential. These local variations in the film-substrate binding energy cause severe local structural distortions related to the actual registry between film and substrate but do not lead to an overall strain, i.e., the oxide film stays incommensurate in one direction.

II. EXPERIMENTAL AND COMPUTATIONAL METHODS

A. Experiment

STM experiments were performed with a homebuilt UHV-STM cooled with liquid helium and operating at $5-6$ K. Topographies shown were obtained in constant-current mode at the mentioned bias voltage of the sample with respect to the tip. The starting point for the preparation of the CoO c(10×2) bilayer on Ir(100) is the clean Ir(100)-(1x1) structure obtained as described in Ref. 22. The base pressure in the preparation chamber is $8\cdot 10^{-11}$ mbar. Cobalt oxide is obtained by depositing 0.9ML Co at 50° C and subsequent oxidation at 250° C in an oxygen atmosphere. The oxygen dose is applied by a needle-valve and a tube roughly 2 mm in front of the surface for 100 s, the total pressure in the chamber during oxidation is $5\cdot 10^{-10}$ mbar ($5\cdot 10^{-8}$ mbar estimated pressure at the sample). Finally the oxide films were post-annealed at 380° C.

B. Theory

The Vienna Ab-initio Simulation Package (VASP)[23,24] in the projector augmented wave (PAW) framework[25] was employed to perform Density Functional Theory (DFT) calculations using the generalized gradient approximation of Perdew-Burke-Ernzerhof (PBE)[26] for the exchange correlation functional. The localized nature of the Co d-states was treated using the GGA+U approach of Dudarev.[27] Testing a range of U parameters, a value of $U-J$=1 eV was found to give the best agreement between the present calculations and experiment.[19] This choice of $U-J$=1 eV is also supported by the calculated bulk volume, which is very close to experiment, and by a satisfactory description of the electronic structure as compared to a more sophisticated, but very costly, approach using hybrid functionals.[28] Hence, if not stated otherwise all results of the present work refer therefore to this choice of $U-J$=1 eV. A repeated slab model was used, consisting of five Ir layers and CoO overlayers on both sides of the Ir slab to avoid dipolar interactions between the repeated slabs separated by a vacuum of 17 Å. In all calculations the structural degrees of freedom are fully relaxed on a Monkhorst-Pack type 4x4x1 k-mesh. The calculations were carried out within a c(10×2) unit cell containing nine oxygen and nine cobalt atoms arranged in a pseudo-hexagonal configuration on top of ten Ir atoms of the first layer (Fig. 1) as suggested by experiment.[18,19] We imposed mirror symmetry in the [011] direction. In the first configuration, termed "mirror top" (MT), the mirror plane contains one Co, one O, and one Ir atom of the first layer (Fig. 1(a)); in the second configuration, termed "mirror bridge" (MB), the mirror plane does not contain an Ir atom of the first layer (Fig. 1(b)). The two configurations differ by a shift of the CoO film with respect to the substrate by half an Ir lattice constant a_{Ir}. However, due to the large unit cell, this shift is equivalent to shifting the film by only $1/18\cdot a_{Ir}=0.15$ Å. STM images simulating the constant current measuring mode of STM were calculated using the Tersoff-Hamann approximation.[29]

III. RESULTS AND DISCUSSION

A. Understanding the elements of the CoO-c(10×2) film structure

In order to test the validity of the structural model proposed by the LEED analysis of Ref. 19 we first discuss the c(10×2) phase in the claimed MT configuration. We performed DFT calculations using the standard PBE functional with two distinct starting configurations: in one case we started with a slightly distorted, but otherwise flat, CoO bilayer that should easily converge into the structure found on Pd(100).[20] In the other case, we modified the above structure to contain two different types of oxygen species (low-lying and high-lying ones mimicking the LEED results[19]) as indicated by the different shading in Fig. 1. The forces acting on all the atoms were minimized in nonmagnetic and spin-polarized calculations for various ferro- and antiferromagnetic (strictly speaking ferrimagnetic) arrangements of the Co atoms.

For the flat oxide model a search for a global energy minimum based on a force minimization was unsuccessful. This finding can be rationalized on the basis of a simplified quasi epitaxial (SQE) model.[21] This model correctly mimics the large corrugation of the O atoms already for much smaller unit cells. Here a distorted flat oxide model can be stabilized, but by overcoming a small energy barrier of less than 0.1 eV (the detailed value depends on the chosen magnetic configuration) the O atoms directly above the Ir substrate atoms find their minimum positions at low distances corresponding to the c(10×2) structure and gain about 110 meV/CoO. Comparing nonmagnetic calculations for the strongly corrugated c(10×2) model with the best metastable flat oxide model, an energy gain of the former of 60meV/CoO was obtained. Quite unexpectedly a ferromagnetic configuration for the strongly corrugated c(10×2)

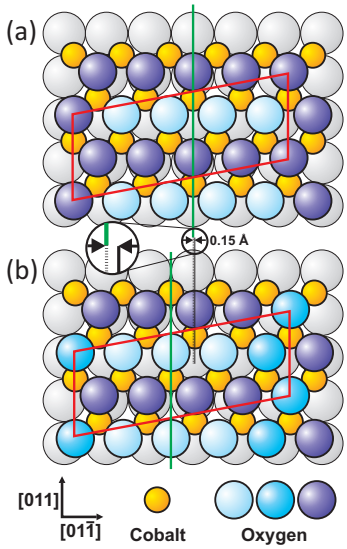

FIG. 1. (Color online) Schematic model of the starting configurations for the calculations. The flat CoO bilayer film with c(10 × 2) periodicity with respect to Ir(100) and a primitive unit cell are displayed. Small yellow (bright) spheres denote cobalt atoms, large blueish (gray) spheres denote oxygen atoms, and even larger light gray spheres denote iridium atoms of the uppermost layer. Oxygen atoms shaded darker are closer to the substrate in the corrugated starting configuration. The unit cell contains 9 Co and 9 O atoms, aligned parallel to the [01$\bar{1}$] directions and perfectly row-matched in the [011] direction. (a) The registry of the film is chosen symmetric to a first layer Ir top site, i.e., there is a mirror plane (green line) intersecting a Co, an O, and a first layer Ir atom ("mirror-top" (MT) model). (b) Same as (a) but with ∼0.15 Å lateral shift of the CoO with respect to the substrate. The film is now symmetric to a *first* layer Ir bridge site, i.e., the mirror plane intersects a Co, an O, and a *second* layer Ir atom ("mirror-bridge" (MB) model).

model could not be stabilized by force minimization. However, with some of the Co species antiferromagnetically coupled (for details see below), a stable minimum appeared with a total energy lower by 110 meV/CoO compared to the best intermediate ferromagnetic solution. The structural parameters that resulted had an average mean square deviation of 0.067 Å between experiment[19] and a standard PBE calculation considering the of 58 parameters of the structure. However, the lateral deviations are largely due to the difference between the theoretical (3.88 Å) and experimental (3.84 Å) Ir lattice constants; correcting for this difference by rescaling the DFT structural parameters, the standard deviation is reduced considerably to 0.037 Å. Thus, we clearly support the published model and rule out the possibility that a gentle corrugation of the CoO film as reported for Pd(100)[20] might also occur for Ir(100).

We investigated the influence of the choice of $U-J$ on the predicted results as compared to the experiment, in particular the vertical height of the Co and O atoms (Fig. 2). Consistent with other DFT+U studies for ultra-thin oxide films on metal supports[30,31], we find that smaller $U-J$ parameters compared to bulk oxides have to be chosen to describe the properties of the film correctly. Even for the complete neglect of on-site Co d correlation effects in the calculations (PBE), the experimental values are well reproduced. The closest match, however, is achieved for the choice of a rather moderate $U-J$=1 eV for the Co d electrons. Larger values rapidly worsen the agreement, both in absolute binding distances and in the relative heights of adjacent atoms (buckling directions; see, e.g., the second Co and O atom from the left in Fig. 2). This can be traced back to the stronger localization of the Co d electrons and the accompanying reduction of hybridization with the neighboring atoms. For the $U-J$=1 eV calculation the mean square deviation between LEED and DFT data amounts to only 0.02 Å in vertical and 0.03/0.07 Å in lateral x/y CoO (lattice constant corrected) positions. The positions of the Ir atoms are almost identical within a standard deviation of 0.01 Å and 0.02 Å in lateral (lattice constant corrected) and vertical positions, respectively. The total mean-square deviation for all 58 parameters is now 0.033 Å. Therefore, the geometrical structure obtained from our DFT+U calculations quantitatively agrees with the published experimental data. Fig. 3 shows the resulting structure in MT and MB symmetry in a ball model with layer distances and corrugation amplitudes included. All atomic coordinates of the relaxed structure according to the $U-J$=1 eV calculation are tabulated together with the experimental values from Ref. 19 in the Appendix.

As previously mentioned, antiferromagnetically coupled cobalt atoms turned out to be an essential ingredient in the MT structure. The structure with the lowest energy is that in which the Co atoms located near bridge positions form an antiferromagnetic chain segment, whereas the Co atoms near hollow positions form a ferromagnetic chain segment along the [01$\bar{1}$] direction of the substrate (Fig. 3 (a)).[21] Locally, this magnetic structure exhibits the same

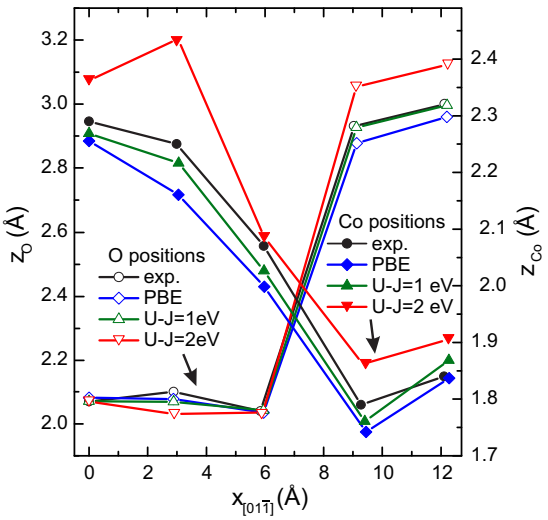

FIG. 2. (Color online) Vertical coordinates of Co and O atoms parallel to the [01$\bar{1}$] direction for different values of $U-J$ in the DFT+U calculations. Closed symbols denote the vertical positions of the Co atoms (left axis), open symbols those of the O atoms. The experimentally determined values from Ref. 19 are plotted for comparison. Only the positions in one half of the MT unit cell are shown.

zig-zag arrangement of parallel spins along the [011] direction as was reported for the (9x2) structure of CoO on Pd(100) (AFM3 structure of Ref.20). However, due to the odd number of Co ions within the unit cell, no complete antiferromagnetic configuration can develop here.

The magnetic configuration has considerable influence on the structure as demonstrated in Fig. 4. In order to be compatible with a non-magnetic calculation, the magnetic configurations here are determined by a standard PBE calculation, which is already rather close to the best DFT+U structure (Fig. 2). Quite clearly, the strong corrugation of the structure is also present in a non-magnetic calculation, but the inclusion of magnetism is absolutely necessary to capture the essentials of the experimental data, particularly for the Co atoms, but also for the high-lying oxygen atoms. Aside from the smaller size of a nonmagnetic Co atom, the corrugation along the Co chains is too soft, while the opposite is true for the high-lying oxygens. On the other hand flipping the spins of Co1 and Co2 (see Fig. 3 (a)) in the antiferromagnetic chain segments also has a non-negligible effect on the vertical distances as seen by comparing the curves "mag." and "mag. alt." which represent the magnetic configurations shown in Fig. 3 without and with flipped spin of Co1 and Co2. Although the "mag. alt." configuration is the next stable configuration, visual inspection clearly shows that the experimental trends are less well reproduced. A spin flip between Co1 and Co2 also strongly influences Co4 via interaction with the connecting oxygen atoms.

We discuss now possible driving forces for the enormous rumpling of the cobalt oxide film. In the [011] direction the film expands slightly (4% with respect to a bulk CoO(111) bilayer) to accomplish row-to-row matching with the Ir substrate. Consequently along the [01$\bar{1}$] direction the Co atoms are aligned roughly in between the first layer Ir rows with lateral positions gradually altering from (near) hollow to (near) bridge positions. Their vertical positions vary by about half an Ångstrøm in order to keep similar bond lengths to the substrate atoms. Four of the oxygen atoms are found far above the narrow triangular Co sites, similar to their position in a rocksalt CoO lattice. The other five oxygen atoms — in particular those near top positions of the outermost Ir layer — are found to dive right into the Co layer thus locally forming a planar bonding configuration similar to the hexagonal boron-nitride structure. To allow for this the adjacent Co atoms have to give way via lateral, concerted movements increasing the size of the triangular site by as much as 50%. The "low-lying" oxygen atoms come to rest almost 1 Å closer to the surface than the "high-lying" ones. The strong chemical interaction of the low-lying oxygen atoms with the Ir atoms is indicated by the small atomic distances of about 2.1 Å which lie in the range of an Ir-O covalent bond (for Ir(100)-(2×1)-O values of $d_{\mathrm{O-Ir}}$=1.95 Å for bridge-bonded oxygen[32] and 1.76 Å and 2.17 Å for bridge and hollow site adsorption[33] are reported), and also by the slight lateral and vertical displacement of the Ir atoms towards the low-lying oxygen atoms.

The driving forces causing the enormous height differences in the oxygen layer can be created either in the film or by the interface. In the first possible scenario the high-lying oxygen atoms (in conjunction with locally rather unspecific Co-Ir bonds) cause trimerization within the Co lattice and consequently the remaining O atoms "sink" into the widened hollow sites. The second possible scenario is that very site-specific Co-Ir bonds facilitate local

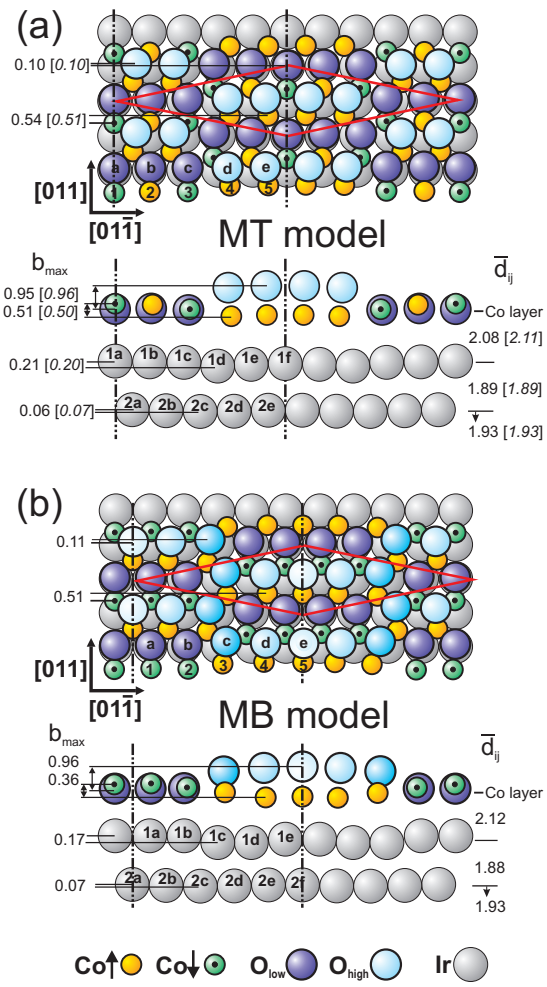

FIG. 3. (Color online) Top and side views of the CoO-c(10 × 2) Ir(100) (a) MT and (b) MB structure including structural parameters and spin orientations as determined by the DFT+U calculations. (Experimental values taken from Ref. 19 are given in brackets.) The different types of atoms are displayed as in Fig. 1 and the magnetization direction of the Co atoms is indicated by different coloring and a dot for the *down* configuration. Oxygen atoms near Ir top sites (shaded darker) lie between the Co layer, while those in the vicinity of Ir bridge positions (shaded lighter) occupy sites above the Co atoms.

narrowing and widening of the cobalt lattice and/or the additional binding of an oxygen atom to an Ir top site is so energetically favorable that it overcompensates the strain energy created in the film. The first scenario does not appear to be supported by experimental evidence or the theoretical calculations: Since the trimerization is associated with a binding potential within the film the same should in fact happen on the Pd(001) surface, which is not observed experimentally.[20] Furthermore, such a trimerization should smoothly (i.e., without activation barrier) evolve from the flat film configuration, which is not supported by the DFT calculations.

Conversely, the second scenario directly relies on the specific binding properties of the film to Ir(100), which easily might be different than for Pd(100), for example. The additional O-Ir bond can also account for the formation of an activation barrier for reaching the BN-like configuration, since the film distortion has to proceed at least partly *before* the O atoms can gain significant energy from the Ir-binding. In order to evaluate whether the covalent Ir-O bond would be able to provide enough energy to drive the whole local rearrangement, we determined the energy required to remove either a low- or high-lying oxygen by taking one of them out of the slab with all other atoms frozen at their former positions. The low-lying oxygen are not stronger bound than the high-lying ones but weaker by about 0.4 eV. That means the O-Ir bond will certainly contribute to the energy balance, but it cannot be the decisive factor for the local restructuring. The penalty for distorting the film and for the smaller oxygen binding energy must be overcompensated by an energy gain from the moving Co atoms (when we suppose that the binding energy of the high-lying oxygen atoms are only negligibly affected by the rearrangement). In the next section we will show how this scenario is also supported by the evaluation of the atoms' potential landscapes in the structure.

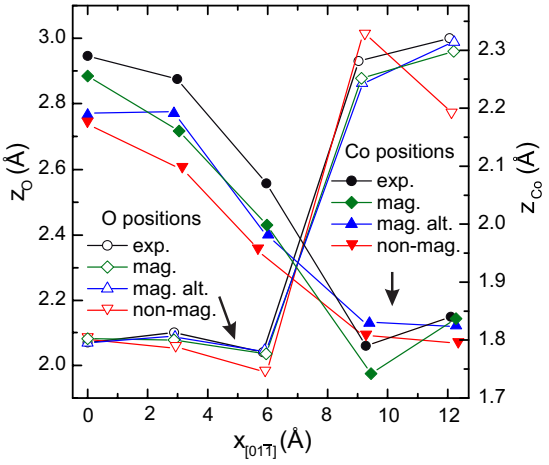

FIG. 4. (Color online) PBE calculated vertical coordinates of Co and O atoms for different magnetic configurations parallel to the [01$\bar{1}$] direction. Closed symbols denote the vertical positions of the Co atoms (right axis), open symbols those of the O atoms. "Non-mag." refers to a nonmagnetic calculation, "mag." to the magnetic configuration shown in Fig. 3, and "mag. alt." to the same configuration but with the spins of Co1 and Co2 switched. The experimentally determined values from Ref. 19 are plotted for comparison. Only the positions in one half of the MT unit cell are shown.

B. Registry of film and substrate – Moiré structure

Considering the rather unspecified local positions of cobalt and oxygen species with respect to the substrate, we have tested whether the chosen "mirror-top" (MT) registry (Fig.1(a)) between the film and the substrate is energetically distinguished from the "mirror-bridge" (MB) model with a close lying alternative registry of the CoO film. In the MB model the film is nominally shifted by half a lattice parameter $a_{\mathrm{I}r}$ of the substrate. However, since the Co and oxygen atoms in the structure already sample 9 different positions within the Ir unit cell, the MT and MB configurations are related by effectively shifting the CoO film as little as $1/18 \times a_{\mathrm{I}r} \approx 0.15$ Å (cf. Fig. 1b). Therefore it is not surprising that after proper relaxation a structure results (cf. Fig. 3(b) and Appendix) which is approximately energetically degenerate with the former one (ΔE = -6 meV/CoO for DFT+U and 9meV/CoO for PBE). The local binding configurations (rock salt or h-BN) are found to be rather similar in both structures. However, due to the different position of the mirror plane, symmetry now enforces an odd number (three) of high-lying oxygen atoms. Additionally, there are two more oxygen atoms in a medium high and only the remaining four in a "low-lying" position. In the MB configuration the near-hollow Co atoms are ferromagnetically ordered as for the MT registry. However, now also the near-bridge Co atoms are ferromagnetically ordered with an antiferromagnetic coupling between the two groups (Fig. 3). This indicates that there is a strong ferromagnetic coupling induced by the substrate, which is strongest for the Co atoms in hollow sites. On the other hand, for the near-bridge site Co atoms, the ferromagnetic coupling is weakened and oxygen-mediated antiferromagnetic coupling can compete. (See results and discussion on the SQE models in Ref. 21.) Symmetry imposes an additional constraint: In the MB model, symmetry requires an even number of Co atoms with reduced ferromagnetic coupling; hence, they cannot couple antiferromagnetically towards the ferromagnetic segments on *both* sides. Obviously, the magnetic mismatch at one side towards an adjacent ferromagnetic segment is so much less favorable that the antiferromagnetic coupling of ferromagnetic Co blocks in the [011] direction wins over the combination of ferromagnetic and antiferromagnetic stripes.[21]

In order to reveal how the two limiting configurations of the c(10 $\times$ 2) structure of CoO/Ir(100) will appear in STM images we have calculated topographic images (Fig. 5). It turns out that for all bias voltages and distances the high-lying oxygen atoms dominate the images with well-separated quadrumers or trimers of protrusions for the MT- or MB-phase respectively. This finding clearly disproves the tentative assignment offered by Giovanardi et al.[18] that the protrusions observed in STM images are related to Co atoms. For small tip-sample distances the highest-lying Co atoms near bridge positions become visible as well and in the case of the MB configuration also the "medium-high" oxygen atoms appear as much smaller protrusions, forming zig-zag-like rows in between the trimer arrays. The contribution from the Co atom become more obvious when imaging one of the rare single oxygen vacancies (cf., inset of Fig. 5(h)).

An almost quantitative agreement between experiment and theory is reached for the MB structure, while the MT structure agrees qualitatively concerning the bright features of the oxygen atoms for both bias voltages. The main differences between the calculations and experiment are the reduced brightness at the MT mirror plane and increased

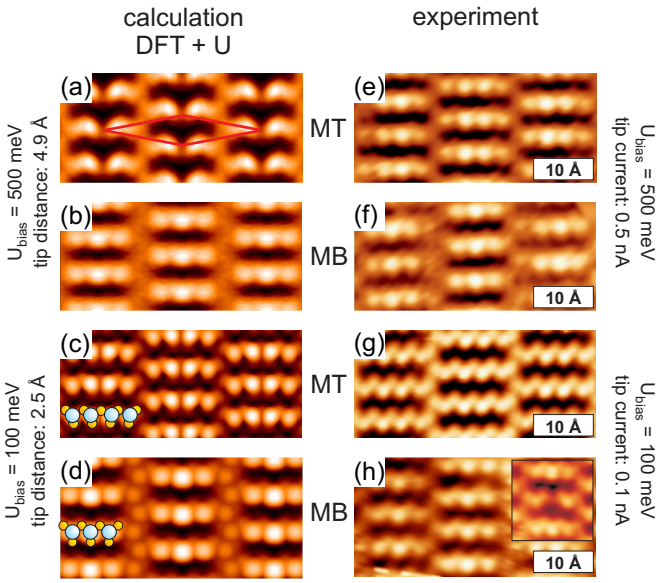

FIG. 5. (Color online) Left: calculated STM images for the MT and MB-configurations of the CoO film for two different bias voltages and tip-surface distances. Right: Corresponding experimental STM images taken at the given tunneling parameters. The inset in (h) displays a vacancy at the high-lying oxygen site.

weight of the adjacent Co atom in Fig. 5(a) and the generally increased weight of the Co atoms in the experimental images at low bias (Fig. 5(g), (h)). The slight discrepancy between Fig.5(a) and (e) can be attributed to the different contributions of the Co atoms due to the assumed collinear antiferromagnetic arrangement (see Ref. 21) in this chain segment. A possible non-collinear arrangement of these antiferromagnetic chains suggested by model calculations[21] will lead to a more homogeneous contribution of the Co atoms and improve the agreement with experiment. We attribute the increased weight of the Co atoms in the experimental images at low bias voltages to an effect causing a reduction in dI/dV tunneling spectra at zero bias which is not reproduced by the present calculations. Due to the zero-bias anomaly the tip will move closer to the surface increasing the weight of the Co atoms.

The calculations predict that the CoO film should occur with similar weights in both registries (and possibly even in any registry in between) at the surface. Large-scale, atomically resolved STM images measured at 5 K (Fig.6) indeed show that the "c(10×2)-film" does not consist of coexisting domains of either the MT or MB phase. Instead, already on a 100 Å scale (Fig. 6(a)), we observe an aperiodic variation of the number of maxima (3 or 4) within the "c(10×2) unit cell". Even more, the average repetition length of these multimers determined from STM images like Fig. 6(b) is about 25.5 Å = 9.4 a_{Ir} significantly smaller than the expected $10\,a_{Ir}$ = 27.2 Å. Virtually the same value (25.6 Å) for the (pseudo-)periodicity of this structure has recently been inferred from a careful analysis of high-order LEED spot positions including double diffraction effects.[34]

The whole scenario can easily be explained by a one-dimensionally incommensurate structure, whereby the pseudo-periodicity originates from a Moiré modulation between the two lattices involved (CoO and Ir). The peculiarity of this combination of a hexagonal and a square lattice leads to an anti-correlation of the Moiré modulation between neighboring rows giving rise to a "centered" rectangular unit cell "c(9.4×2)" (which, of course, is a crystallographically incorrect nomenclature). Within one such Moiré periods we have on average 8.4 CoO unit cells aligned along 9.4 Ir cells, which in turn corresponds to an average lattice parameter of 3.04 Å in the $[01\bar{1}]$ direction. This value is 0.9% larger than that of the CoO bulk structure (3.012 Å) and therefore somewhat closer to the second unit vector (3.11 Å), which is 3.3% strained by the row-to-row matching. Since the film is obviously not forced into any commensurate structure, the observed lattice parameter of 3.04 Å in the $[01\bar{1}]$ direction is the free response of the film to the uniaxial expansion in the [011] direction. As a rough estimate, the average of the two orthogonal dimensions of the quasi-hexagon (3.11 Å and 3.04 Å) would correspond to a lattice constant of a hypothetical unstrained film which is about 2% larger than the bulk value. The same expansion was found for the two-dimensional Moiré structure of FeO on Pt(111).[14,15] The experimentally determined average lattice parameter in the $[01\bar{1}]$ direction also deviates as little as 0.8% from that of the c(10×2) coincidence mesh (3.017 Å) and thus is within the accuracy by which DFT and LEED (using a conventional LEED optics) are able to determine equilibrium lattice parameters at all. Hence, the commensurate c(10×2) phase is an excellent model structure, exhibiting all the local features of the real oxide structure fairly well. However, due to the fact that the Moiré period is not a whole multiple of the substrate unit vector, the film's registry will oscillate laterally between the two limiting structural configurations described by the

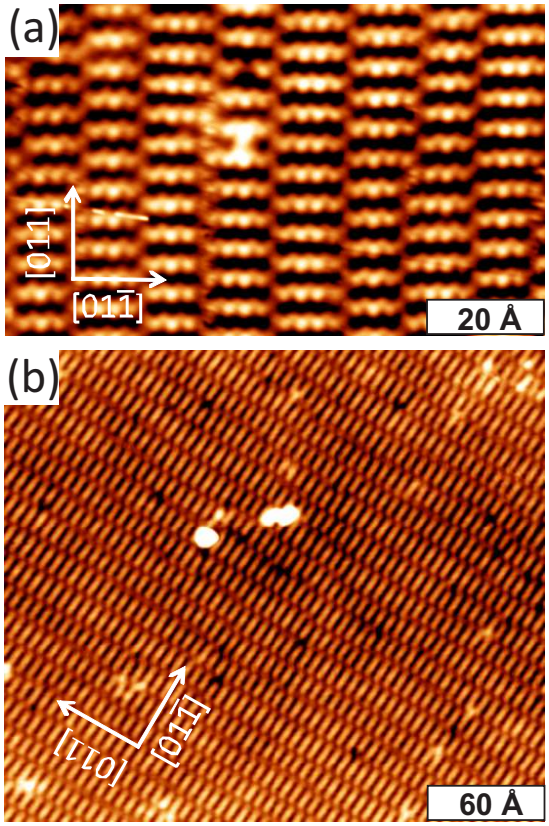

FIG. 6. (Color online) (a) Atomically resolved STM image (100 Å × 60 Å). The CoO film appears inhomogeneous both in the number of maxima and size of apparent unit cells. (b) Large scale STM topography (300 Å × 250 Å) demonstrating the Moiré structure of the CoO film on Ir(100).

MT and MB models.

The Moiré structure, however, is *not* a signature of a laterally unspecific binding potential. In the limit of infinite domain size and assuming an ideal (undistorted) Moiré structure, both the Co and O atoms will assume every local position in the Moiré direction with equal weight, i.e., their probability function will be a continuous trace in three-dimensional space. Any deviation from that continuous trace points to local relaxations that are caused by lateral variations of the binding energy to the substrate. The combined structural parameters of our two model calculations (MB and MT) in reduced coordinates (i.e., modulo a_{Ir}) provide a rather narrow sampling grid of these traces which are displayed in Fig.7 in top and side view. Were the two structures representatives of an ideal Moiré structure, the sampling points for the traces would be equidistant in the horizontal coordinate ([01$\bar{1}$] direction). The local compression of the true atomic coordinates indicates sites of higher binding energy (attraction points), while a local rarefaction denotes energetically unfavorable positions (repulsion points).

For the oxygen trace it can clearly be seen that the near-top position attracts the oxygen atoms both vertically and laterally, indicating a rather sharp minimum of the oxygen binding potential on top of the Ir atoms. Fig.7 shows that there is a rather narrow range smaller than our sampling grid distance in which the oxygen atoms switch from "low" to "high" positions. Due to the exponential distance dependence of the tunneling current in STM, the appearance of oxygen atoms in topographies is limited exclusively to the high-lying oxygen atoms (for not too close tip-sample distances, cf., Fig. 5). From Fig.7 it follows that about 7/18–8/18 of all oxygen species will reside in this range and thus show up in STM as a non-periodic sequence of trimers and quadrumers giving an average of 3.3 - 3.7 protrusions per Moiré cell. This number is in good agreement to the experimental findings (cf., Fig. 6).

For the Co atoms, we find a preference of the near-hollow site where the lateral coordinates accumulate densely, while the near-bridge position appear rather unspecific in energy. The transition range between a position above the rim of an Ir atom and the near-hollow site turns out to be almost completely unwanted. A position within this "repulsion zone" is assumed for only one of the limiting models (MB registry). The occupation of this intermediate site is associated with the occurrence of the "medium-high" oxygen atom as shown by the red dashed triangle in Fig. 7. For the MT registry, the Co atoms directly switch from one type of site to the other within adjacent CoO unit cells as indicated by the solid blue triangles in Fig. 7. Hence, the existence of a Co atom at the intermediate site

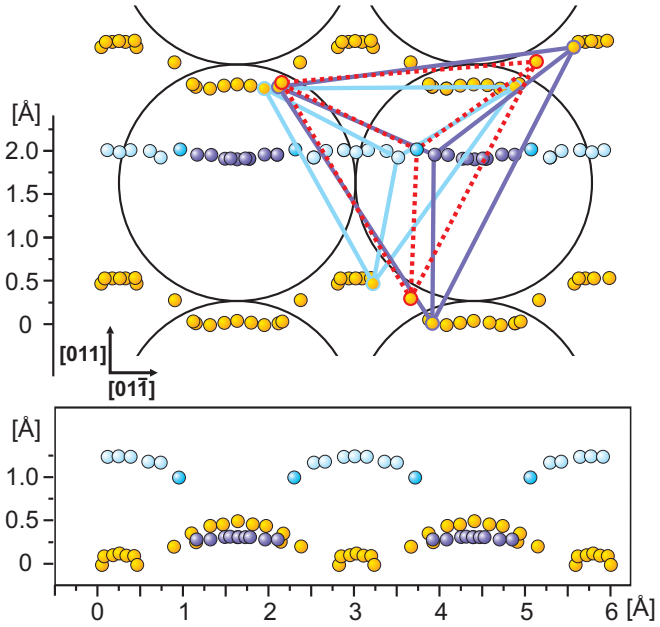

FIG. 7. (Color online) Compilation of reduced atomic coordinates (modulo substrate unit vectors) of Co and O taken from DFT calculations for both registries visualizing the Co and O traces across the Ir(100) unit cell in the Moiré structure. The triangles drawn in denote certain adsorption sites of oxygen (for details see text).

might be a result of the limiting MB registry. Any small disturbance along [01$\bar{1}$] will presumably cause a switch to a more likely site.

IV. CONCLUSION

With the present analysis we have corroborated a previous structural analysis of the bilayer CoO(111) film on Ir(100) by DFT calculations. The calculations support the experimental analysis quantitatively and trace the lateral modulations within the local structure back to the lateral variations of the Co-Ir binding potential in cooperation with an additional O-Ir binding near top Ir sites. The latter is also responsible for an activation barrier that evolves in the structural transition from a flat bulk-like film geometry to the real ground state structure. This activation barrier can also prevent the ground state structures from being found in total energy calculations. Contrary to previous expectations, our calculations show that the structure is energetically degenerate with respect to lateral shifts in the [01$\bar{1}$] direction since the 9 CoO units on a 10 units Ir coincidence mesh already samples the local sites on a grid of only 0.3 Å in this direction. Hence, any such lateral displacement of the film can shift the sampling grid by at maximum 0.15 Å against the former situation. However, this variability against displacement does not imply, as sometimes erroneously concluded, that the binding towards the substrate must be laterally unspecific, which is definitively not the case for the present system; rather, only the *average* of the binding energy over all sampled positions remains independent of lateral shifts of the structure.

An important and further implication of this fact is that there is no driving force for the film to enter a commensurate structure with a large unit cell. If that unit cell is large enough the total binding energy to the substrate will be indistinguishable from that of the Moié structure, since both sample essentially the same potential landscape. On the other hand, to reach a commensurate structure the film has to accommodate additional strain energy, which disfavors this process. This general prediction is impressively verified by large scale atomically resolved STM topographies, which clearly reveal one-dimensional incommensurate Moiré structures with a period of about 9.4 a_{Ir}, rather than a commensurate c(10 × 2) or (9 × 2) phase. Since the film always remains in a long-range relaxed state, the lattice parameter assumes its "natural" value, which for ultra-thin films might be different than bulk. In the present system this condition is only fulfilled in one dimension since the CoO film still suffers from a uniaxial tensile strain due to the row-on-row matching in [011] direction. Hence, it will react with an accordingly reduced lattice parameter (with respect to the "natural" one) in the non-strained Moiré direction.

A compilation of structural parameters from DFT calculations for two limiting commensurate structures provides us with a rather narrow sampling grid for the local film structure as a function of the current registry to the substrate

unit cell. The traces of atoms across the substrate unit cell can be regarded as a probability function for the spatial distribution of atoms within the Moiré structure and thus provides a crystallographic description of the system. We identify pronounced attraction and repulsion regions for Co and oxygen positions, reflecting the local variation of the film-substrate interaction potential. The existence of the repulsion zone for the Co atoms locally widens the triangular oxygen sites, thus allowing the oxygen atoms to dive into the Co layer and bind towards Ir atoms. Hence, the location of Co repulsion points determines which oxygen atoms undergo this process. It is therefore more or less by chance that the O-Ir binding proceeds at Ir top positions, though it might be that these positions are indeed rather favorite oxygen docking sites for oxide films. The one-dimensional Moiré structure also has consequences for the magnetic properties of the film. The ferromagnetic coupling between Co species via the Ir substrate is counterbalanced by the antiferromagnetic exchange interaction via oxygen atoms. Local symmetry and binding requirements prevent long-range antiferromagnetic and ferromagnetic structures, and produce a film consisting of groups of ferromagnetically and antiferromagnetically coupled subunits. We speculate that the true magnetic structure might fluctuate with specific local configurations. Spin-polarized STM imaging might be an experimental way to investigate this. Our calculations indicate that the tunneling current is sufficiently spin-polarized in the low-bias region $|V| < 0.4$ eV.

Similar structural configurations are expected to arise in other overlayer systems. The assignment of large commensurate cells might, in fact, be wrong and caused by limited experimental resolution or by observation over limited regions. The message beyond the actual system under investigation – CoO on Ir(100) – is that strong site-dependent binding does not lead to commensurability *per se* nor are incommensurate, non-periodic films free of severe local distortions.

ACKNOWLEDGMENTS

The authors are grateful for the financial support from the Austrian Science Fund (FWF) SFB FOXSI F4511-N16 and the National Science Foundation (DMR-1105839), and for the computer support of the Vienna Scientific Cluster (VSC).

Appendix: Structural Parameters

TABLE I. Structural parameters and magnetic moments for the two limiting structures with different mirror symmetry (MT and MB, see Fig. 1). DFT refers to PBE+U calculations with $U-J$=1 eV. For both DFT models the x/y coordinates in this table have been rescaled to account for the difference between the theoretical and experimental lattice constant (DFT: 3.88 Å, exp: 3.84 Å). The center of gravity of the outermost Ir layer is set to $z = 0.0$. Experimental data of Ref. 19 is shifted accordingly.

	Experiment[19]			MT model (DFT)				MB model (DFT)			
Atom	x	y	z	x	y	z	μ	x	y	z	μ
Co1	0.00	−0.33	2.38	0.00	−0.23	2.35	−2.10	0.16	−0.24	2.32	−2.14
Co2	2.99	−0.32	2.34	3.03	−0.28	2.30	2.18	3.23	−0.23	2.21	−2.19
Co3	5.96	−0.30	2.16	5.91	−0.26	2.11	−2.21	6.15	0.01	2.07	2.20
Co4	9.27	0.16	1.88	9.30	0.20	1.84	2.00	9.33	0.26	1.96	2.13
Co5	12.11	0.18	1.93	12.14	0.26	1.95	2.14	12.22	0.27	1.98	2.16
Oa	0.00	1.54	2.16	0.00	1.63	2.15	0.06	0.09	1.63	2.16	0.06
Ob	2.88	1.62	2.19	2.85	1.63	2.15	0.17	3.02	1.68	2.13	0.06
Oc	5.85	1.61	2.13	5.89	1.68	2.13	−0.10	6.09	1.74	2.85	0.04
Od	9.03	1.62	3.02	9.02	1.65	3.01	0.05	9.16	1.72	3.03	−0.06
Oe	12.06	1.64	3.09	12.09	1.73	3.08	0.08	12.22	1.71	3.09	−0.07
Ir1a	0.00	1.36	0.09	0.00	1.33	0.08	−0.01	0.01	1.33	0.09	−0.05
Ir1b	2.75	1.33	0.06	2.75	1.33	0.07	0.07	2.77	1.35	0.07	−0.05
Ir1c	5.49	1.37	0.04	5.49	1.36	0.06	−0.06	5.45	1.36	−0.08	0.13
Ir1d	8.18	1.35	−0.11	8.16	1.35	−0.13	−0.01	8.13	1.35	−0.07	0.00
Ir1e	10.85	1.36	−0.04	10.85	1.34	−0.03	0.28	10.85	1.34	−0.02	0.05
Ir1f	13.57	1.35	−0.01	13.58	1.34	−0.02	0.09				
Ir2a	1.36	0.03	−1.85	1.36	0.03	−1.86	−0.05	1.36	−0.03	−1.84	−0.06
Ir2b	4.06	0.02	−1.89	4.06	0.03	−1.89	−0.01	4.07	−0.03	−1.86	−0.03
Ir2c	6.79	0.01	−1.92	6.78	0.02	−1.92	−0.03	6.77	−0.02	−1.91	−0.03
Ir2d	9.49	−0.01	−1.91	9.52	−0.02	−1.91	0.04	9.52	0.00	−1.91	−0.02
Ir2e	12.22	−0.01	−1.87	12.23	−0.01	−1.89	0.02	12.23	−0.01	−1.88	0.03
Ir2f								14.93	−0.01	−1.88	0.01

* alexander.schneider@physik.uni-erlangen.de

[1] X. Xie, Y. Li, Z.-Q. Liu, M. Haruta, and W. Shen, Nature **458**, 746 (2009).
[2] Y. Sun, P. Lv, J.-Y. Yang, L. He, J.-C. Nie, X. Liu, and Y. Li, Chem. Commun **47**, 11279 (2011).
[3] M. Ando, T. Kobayashi, S. Iijima, and M. Haruta, Journal of Materials Chemistry **7**, 1779 (1997).
[4] Y. Ding, Y. Wang, L. Su, M. Bellagamba, H. Zhang, and Y. Lei, Biosensors and Bioelectronics **26**, 542 (2010).
[5] M. S. Whittingham, Chemical Reviews **104**, 4271 (2004), http://pubs.acs.org/doi/pdf/10.1021/cr020731c.
[6] V. Skumryev, S. Stoyanov, Y. Zhang, G. Hadjipanayis, D. Givord, and J. Nogues, Nature **423**, 850 (2003).
[7] N. Nilius, Surface Science Reports **64**, 595 (2009).
[8] F. P. Netzer, F. Allegretti, and S. Surnev, Journal of Vacuum Science & Technology B: Microelectronics and Nanometer Structures **28**, 1 (2010).
[9] F. P. Netzer, Surface Science **604**, 485 (2010).
[10] W. Meyer, D. Hock, K. Biedermann, M. Gubo, S. Müller, L. Hammer, and K. Heinz, Phys. Rev. Lett. **101**, 016103 (2008).
[11] G. Vurens, V. Maurice, M. Salmeron, and G. Somorjai, Surface Science **268**, 170 (1992).
[12] M. Ritter, H. Over, and W. Weiss, Surface Science **371**, 245 (1997).
[13] S. Shaikhutdinov, M. Ritter, and W. Weiss, Phys. Rev. B **62**, 7535 (2000).
[14] L. R. Merte, L. C. Grabow, G. Peng, J. Knudsen, H. Zeuthen, W. Kudernatsch, S. Porsgaard, E. Lægsgaard, M. Mavrikakis, and F. Besenbacher, The Journal of Physical Chemistry C **115**, 2089 (2011), http://pubs.acs.org/doi/pdf/10.1021/jp109581a.
[15] M. Ritter, W. Ranke, and W. Weiss, Phys. Rev. B **57**, 7240 (1998).
[16] G. Ketteler and W. Ranke, The Journal of Physical Chemistry B **107**, 4320 (2003), http://pubs.acs.org/doi/pdf/10.1021/jp027265f.
[17] F. Li, G. Parteder, F. Allegretti, C. Franchini, R. Podloucky, S. Surnev, and F. P. Netzer, Journal of Physics: Condensed Matter **21**, 134008 (2009).
[18] C. Giovanardi, L. Hammer, and K. Heinz, Phys. Rev. B **74**, 125429 (2006).
[19] C. Ebensperger, M. Gubo, W. Meyer, L. Hammer, and K. Heinz, Phys. Rev. B **81**, 235405 (2010).
[20] L. Gragnaniello, G. Barcaro, L. Sementa, F. Allegretti, G. Parteder, S. Surnev, W. Steurer, A. Fortunelli, and F. P. Netzer, The Journal of Chemical Physics **134**, 184706 (2011).
[21] F. Mittendorfer, M. Weinert, R. Podloucky, and J. Redinger, Phys. Rev. Lett. **109**, 015501 (2012).
[22] D. Lerch, A. Klein, A. Schmidt, S. Müller, L. Hammer, K. Heinz, and M. Weinert, Phys. Rev. B **73**, 075430 (2006).
[23] G. Kresse and J. Hafner, Phys. Rev. B **47**, 558 (1993).
[24] G. Kresse and J. Furthmüller, Computational Materials Science **6**, 15 (1996).
[25] G. Kresse and D. Joubert, Phys. Rev. B **59**, 1758 (1999).
[26] J. P. Perdew, K. Burke, and M. Ernzerhof, Phys. Rev. Lett. **77**, 3865 (1996).
[27] S. L. Dudarev, G. A. Botton, S. Y. Savrasov, C. J. Humphreys, and A. P. Sutton, Phys. Rev. B **57**, 1505 (1998).
[28] C. Rödl, F. Fuchs, J. Furthmüller, and F. Bechstedt, Phys. Rev. B **79**, 235114 (2009).
[29] J. Tersoff and D. R. Hamann, Phys. Rev. B **31**, 805 (1985).
[30] G. Barcaro, I. O. Thomas, and A. Fortunelli, The Journal of Chemical Physics **132**, 124703 (2010).
[31] M. Gubo, C. Ebensperger, W. Meyer, L. Hammer, K. Heinz, F. Mittendorfer, and J. Redinger, Phys. Rev. Lett. **108**, 066101 (2012).
[32] K. Johnson, Q. Ge, S. Titmuss, and D. A. King, The Journal of Chemical Physics **112**, 10460 (2000).
[33] D. Sander, H. L. Meyerheim, Z. Tian, L. Niebergall, N. N. Negulyaev, K. Mohseni, V. S. Stepanyuk, R. Felici, and J. Kirschner, Phys. Rev. B **81**, 153403 (2010).
[34] M. Gubo, *Epitaktische Kobaltoxid-Filme auf Ir(100)* (Verlag Dr. Hut, München, 2011).